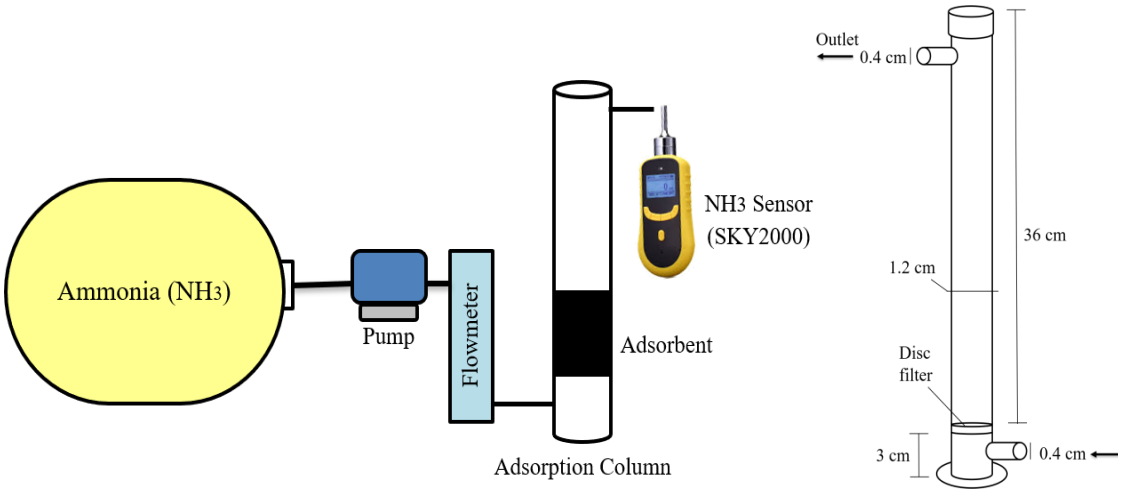

Figure 1. Illustration of the adsorption system test

The variations used in NH_3 adsorption process were adsorbent mass (1, 3, and 5 g) and initial NH_3 concentrations (10±1, 20±1, and 40±1ppm). Data were collected twice for each variation and the adsorption capacity was calculated using equation 4 (Choo et al., 2013):

$$q\left(\frac{mg}{g}\right) = \frac{(C_0 - C_t)\ mg/L \times Flowrate\ (L/min) \times t\ (min)}{Adsorbent\ mass\ (g)} \quad (4)$$

Where; t is the equilibrium time, C_0 and C_t are the gas inlet and outlet concentrations.

Activated carbon used in this study were disposed to the waste management and treatment facility by following applicable rules or can be regenerated using thermal, steam, and chemical processes (Reza et al., 2020).

3. RESULTS AND DISCUSSION

3.1 BET analysis and activation time selection

Microporosities and surface area are important properties that characterize carbon adsorbents (Saputro et al., 2020). The results of BET analysis at various activation times are shown in Figure 2.

Figure 2 shows that the surface area increased from 39.06 m^2/g to 588.41 m^2/g with activation times of 15 and 120 min, respectively, and then decreased to 535.62 m^2/g with longer activation time (180 min). In the activation process, superheated CO_2 diffuses into the inner precursor which burns the blockage of the byproducts, expands the pore, and increases the surface area (Lan et al., 2019; Yuliusman et al., 2017). The activation reaction can be seen below (Cheremisinoff dan Ellerbusch, 1978).

$$CO_2 + C_x \rightarrow 2CO + C_{x-1} \quad (5)$$

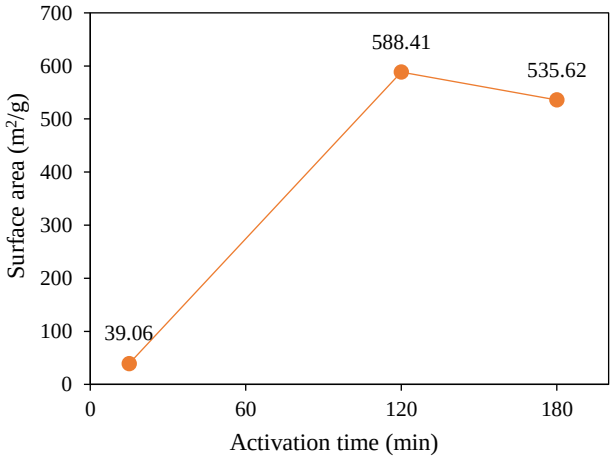

Figure 2. MP-AC surface area at various activation times.

According to Yang and Lua (2003), the increase in activation time increases the BET surface area. However, it can also result in the excessive carbon-CO_2 reaction, thus causing the expansion of the pores and some pore walls to collapse. Therefore, the surface area decreases in 180 min, and 120 min was chosen as the optimum activation time used in this study. The surface area obtained is smaller compared to the previous MP-AC studies using steam and chemical activation (Mukti et al., 2015; Nasrullah et al., 2019), probably due to the temperature and activating agent being used (Gebreegziabher et al., 2019). However, the surface area of activated carbon usually ranges 300-2,000 m^2/g (Saputro et al., 2020), meaning that the result is still in the suitable range.

The isotherm graph obtained (Figure 3) showed the BET type 1 according to IUPAC classification, which usually indicates that the material is micro-shaped (Ambroz et al., 2018) with a relatively broad range of pore size distributions including wider and

narrower micropores (<~2.5 nm) (Giraldo and Moreno-Pirajan, 2018).

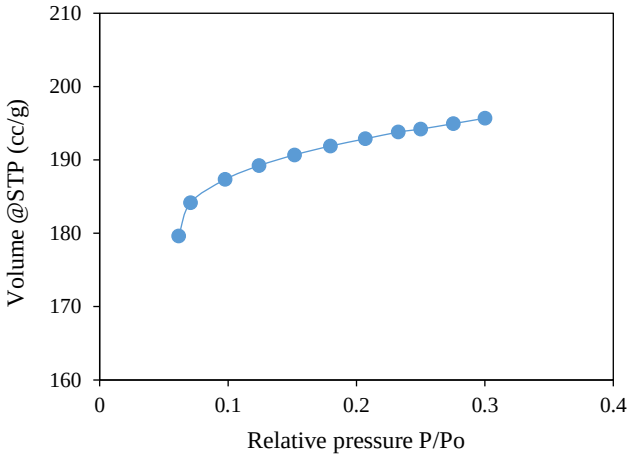

Figure 3. BET isotherm graph

3.2 Characterization of mangosteen peel activated carbon

The results of moisture, ash content, and iodine number compared to other studies are shown in Table 1.

Based on Table 1, the moisture content (6.07%) is higher than other studies' which use chemical activation, and lower than that of using physicochemical activation. This content indicates the hygroscopic nature which can affect the adsorption capacity (Hastuti et al., 2015). Meanwhile, the ash content which indicates the mineral content in activated carbon (Hastuti et al., 2015) has the highest value (9.8%) of all. According to Rangabhashiyam and Balasubramanian (2019), it can be influenced by the pyrolysis temperature and the activation method. The physical activation has a lower efficiency in reducing the mineral content than chemical activation, so the ash content becomes relatively higher.

Table 1. Characterization of MP-AC

Activation/temperature (°C)	Moisture content (%)	Ash content (%)	Iodine number (mg/g)	References
Physical CO_2/850	6.07	9.8	1153.69	This research
Chemical $ZnCl_2$ 600	4.8	1.45	N/A	Nasrullah et al. (2019)
Chemical $ZnCl_2$	1.07	5.68	820	Rattanapan et al. (2014)
Physicochemical KOH-CO_2/828	9.08	1.63	N/A	Ahmad and Alrozi (2010)

The iodine number obtained is 1153.69 mg/g, higher than that of Rattanapan et al. (2014). This iodine number shows adsorption ability, illustrates the porosity of activated carbon, and its higher value attributed to the presence of micropores as already proven in the BET isotherm graph. The result is also included in the range of suitable activated carbon (500-1,200 mg/g) (Saka, 2012).

3.3 FTIR and SEM-EDS analyses

The surface functional group of MP-AC is characterized using FTIR as seen in Figure 4.

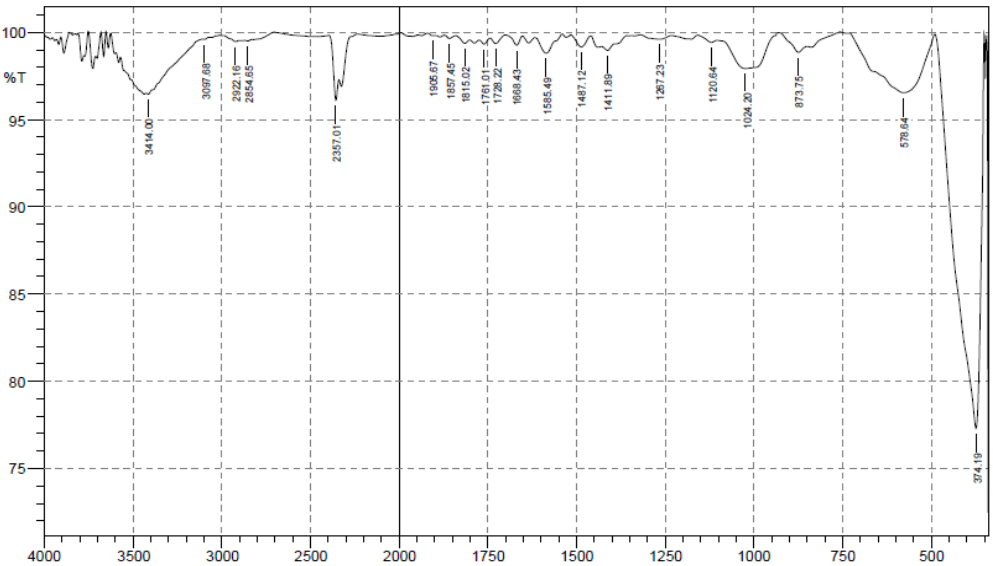

Figure 4. FTIR characterization spectrum of MP-AC

The FTIR result (Figure 4) shows many peaks which representing the complex nature of MP-AC (Nasrullah et al., 2019). The broad peak in 3,600-3,200 cm^{-1} indicates the presence of hydroxyl (O-H) group influenced by CO_2 as an activating agent, and the peak in 2,400-2,300 cm^{-1} shows a formation of nitrile (C≡N) (Ahmad et al., 2013). The small peak that occurs in 1,267.23 cm^{-1} and 1,120.64 cm^{-1} indicates the MP-AC contains a lack of C-O stretching as oxygen functional group in lactonic groups, alcoholic groups, and carboxylate moieties (Chen et al., 2011; Nasrullah et al., 2019). Moreover, the peaks in range of 1,620-1,400 cm^{-1}, 1,760-1,690 cm^{-1}, 3,100-2,850 cm^{-1}, and <900 cm^{-1}, indicates C=C stretching, carbonyl group C=O, hydrocarbons C-H, and aromatic bond C-H, respectively (Ahmad et al., 2013).

The results of SEM analysis before and after the adsorption process can be seen in Figure 5 as follows

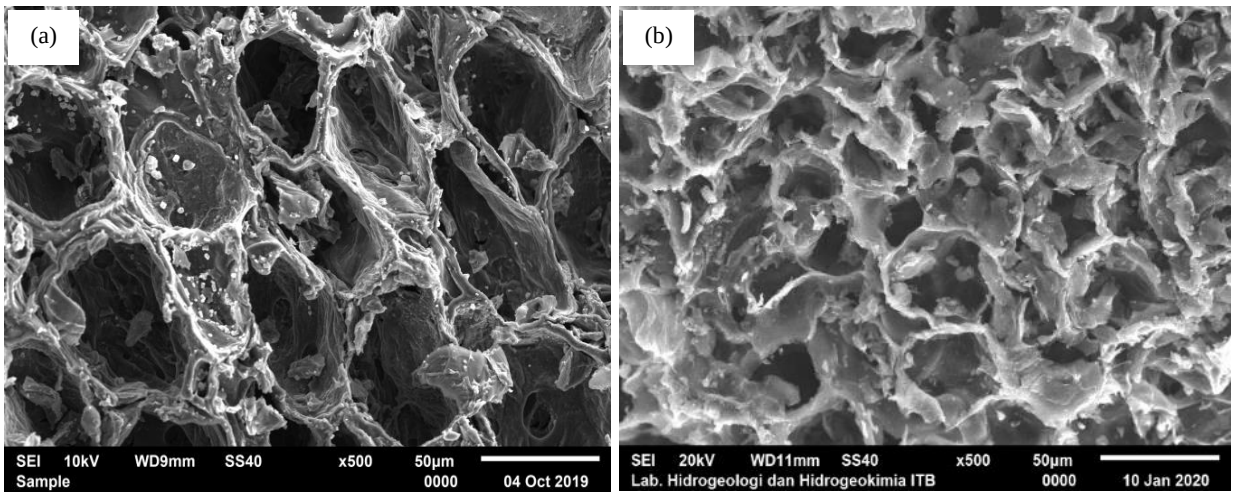

Figure 5. SEM image (a) before; (b) after NH_3 adsorption

Before adsorption (Figure 5(a)), morphology shows presence of circular pores in different size and crevices after the carbonization and CO_2 activation. It is shown that the MP-AC has porous nature that might affect the adsorption process (Nasrullah et al., 2019). After the adsorption (Figure 5(b)) there is an increase of impurities on MP-AC surface compared to the initial sample. This is because the adsorbate moves into the carbon pores during adsorption and results in the pore blockage (Basrur and Bhat, 2018). The surface elements of MP-AC determined using EDS is presented in Table 2.

Table 2. EDS analysis result of MP-AC before and after NH_3 adsorption

Sample	% mass			
	C	N	O	Other compounds
Before adsorption	71.84	16.07	8.77	3.32
After adsorption	70.62	16.94	9.43	3.01

Based on Table 2, the major compounds of MP-AC surface are carbon (71.84%), nitrogen (16.07%), and oxygen (8.77%). The N value of activated carbon is higher than dried mangosteen peel (1-2.67%) (Devi et al., 2014; Giraldo and Moreno-Pirajan, 2018; Nasrullah et al., 2019), probably due to the use of N_2 as the inert atmosphere during the pyrolysis and cooling processes (Ahmad et al., 2013). Meanwhile, after the adsorption, there is no significant difference to these three major compounds.

3.4 Adsorption of NH_3

3.4.1 Effect of adsorbent mass and adsorbate concentration

The breakthrough curves of NH_3 adsorption at different adsorbent mass and adsorbate inlet concentration are presented in Figure 6.

Based on Figure 6, initially, NH_3 is fully adsorbed and adsorption process decreases with approaching equilibrium and gradually becomes constant. Figure 6(a) shows that for adsorbent mass of 1, 3, and 5 g, the equilibrium time was 16, 23, and 25 minutes respectively, indicating that saturation time becomes longer with the addition of adsorbent mass. This is due to the increasing surface area and available adsorption sites (Patel, 2019). Meanwhile, shown in Figure 6(b), smaller inlet concentrations produce the

longer breakthrough curves. According to Ding and Liu (2020) the decreasing inlet concentration decreases the amount of gas molecule passing the adsorbent, so the active sites are exhausted slowly.

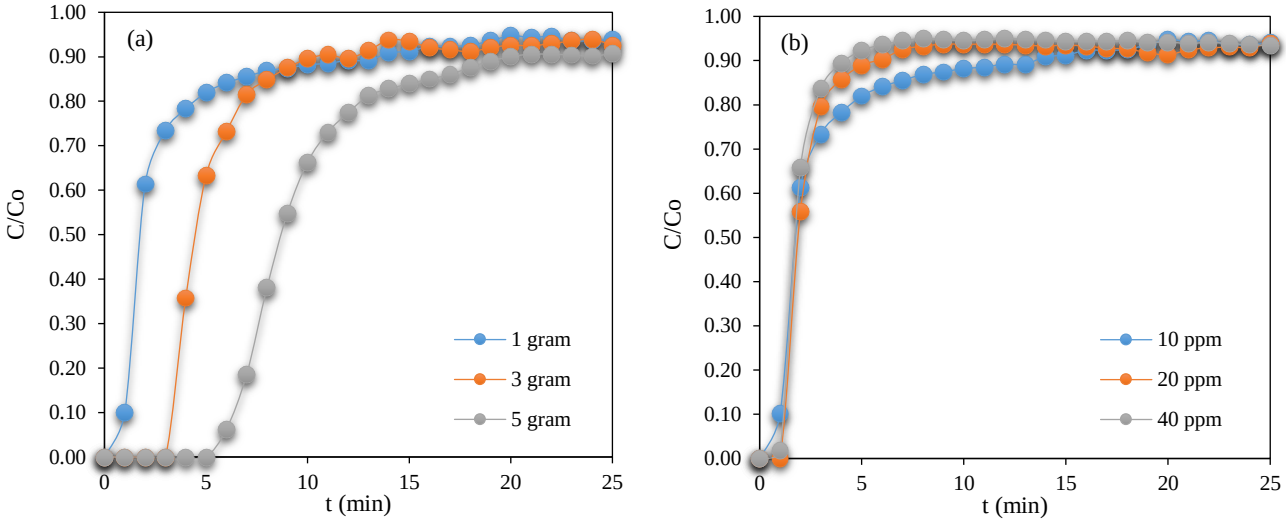

Figure 6. NH_3 breakthrough curve at different (a) adsorbent mass (10 ppm inlet concentration), and (b) different inlet concentration (adsorbent dosage 1 g/27.5 L)

3.4.2 Adsorption capacity

The adsorption capacity value is obtained from the breakthrough graph (Figure 6) which is calculated using Equation 4. The average NH_3 adsorption capacity on MP-AC is 0.41 mg/g. The value is lower compared to commercial activated carbon which ranges from 0.6 to 4.7 mg/g (Ro et al., 2015). This result correlates with the EDS result that the N compounds after and before adsorption do not show significant differences. The NH_3 adsorption may be affected by several factors such as surface functional group, pore size and structure, and surface area (Kang et al., 2020; Yeom and Kim, 2017). Suspected in this study, acidic oxygen functional groups such as –OH, –NH, –C=O, –COOH, and metal ions is the main factor affecting adsorption capacity (Ro et al., 2015; Kang et al., 2020). According to the FTIR result, some of acidic surface oxygen groups are present such as –OH and –C=O. However, the nitrile group is also found, thus increasing the basic nature of the activated carbon, as supported from the EDS result that the %mass of nitrogen can increase the basicity of the activated carbon (Ahmad et al., 2013). This finding might indicate that the surface of MP-AC is less acidic in nature due to the use of physical activation method (Nowicki et al., 2015) thus affecting the adsorption capacity. Additionally, further research is needed to enhance the NH_3 adsorption capacity and the use in numerous environmental applications.

3.4.3 Adsorption kinetics

Lagergren pseudo-first and pseudo-second order kinetic models are evaluated to describe the mechanism of NH_3 adsorption due to their good applicability in most cases (Ghasemi et al., 2014). The equations of pseudo-first order and pseudo-second order can be expressed as follows (Lagergren, 1898; Ho and McKay, 1999);

$$q_t = q_e[1 - e^{(-kt)}] \quad (6)$$

$$q_t = \frac{k_2 q e^2 t}{1 + k_2 q e^2 t} \quad (7)$$

Where; q_e and q_t (mg/g) are the adsorption capacity at equilibrium and time t, respectively; k and k_2 is the pseudo first and second order rate constant, respectively.

The results of kinetic parameters for each kinetic model are presented in Table 3.

For determining the appropriate kinetic model, calculated q_e and R^2 values should be taken into account (Unugul and Nigiz, 2020). According to the results in Table 3 and Figure 7, both pseudo-first order and pseudo-second order kinetic models show high and good R^2 values. However, from the calculated q_e value, the pseudo-first order kinetic model is close to the experiment data. This indicates that the pseudo-first order kinetic model is more suitable to describe the adsorption mechanism where NH_3 adsorption is

physically controlled. The physisorption occurs due to the Van der Waals forces (Guo et al., 2005) and in the pore surfaces which contain hydroxyl group as a preferred site to bind NH_3 (Yeom and Kim, 2017).

Table 3. Kinetics parameter of NH_3 adsorption on MP-AC

Mass (g)	Co (ppm)	qe exp (mg/g)	Pseudo-first order			Pseudo-second order		
			k_1 (min^{-1})	qe_1 (mg/g)	R^2	k_2 (g/min.mg^{-1})	qe_2 (mg/g)	R^2
1	10	0.413	0.205	0.404	0.971	0.394	0.516	0.986
	20	0.303	0.565	0.290	0.991	1.909	0.347	0.999
	40	0.316	0.793	0.309	0.996	2.507	0.370	1.000
3	10	0.363	0.231	0.345	0.988	0.619	0.417	0.992
	20	0.450	0.201	0.475	0.996	0.259	0.650	0.992
	40	0.448	0.306	0.474	0.993	0.415	0.637	0.987
5	10	0.427	0.134	0.441	0.994	0.204	0.586	0.986
	20	0.493	0.124	0.581	0.989	0.106	0.857	0.983
	40	0.515	0.169	0.612	0.989	0.135	0.908	0.984

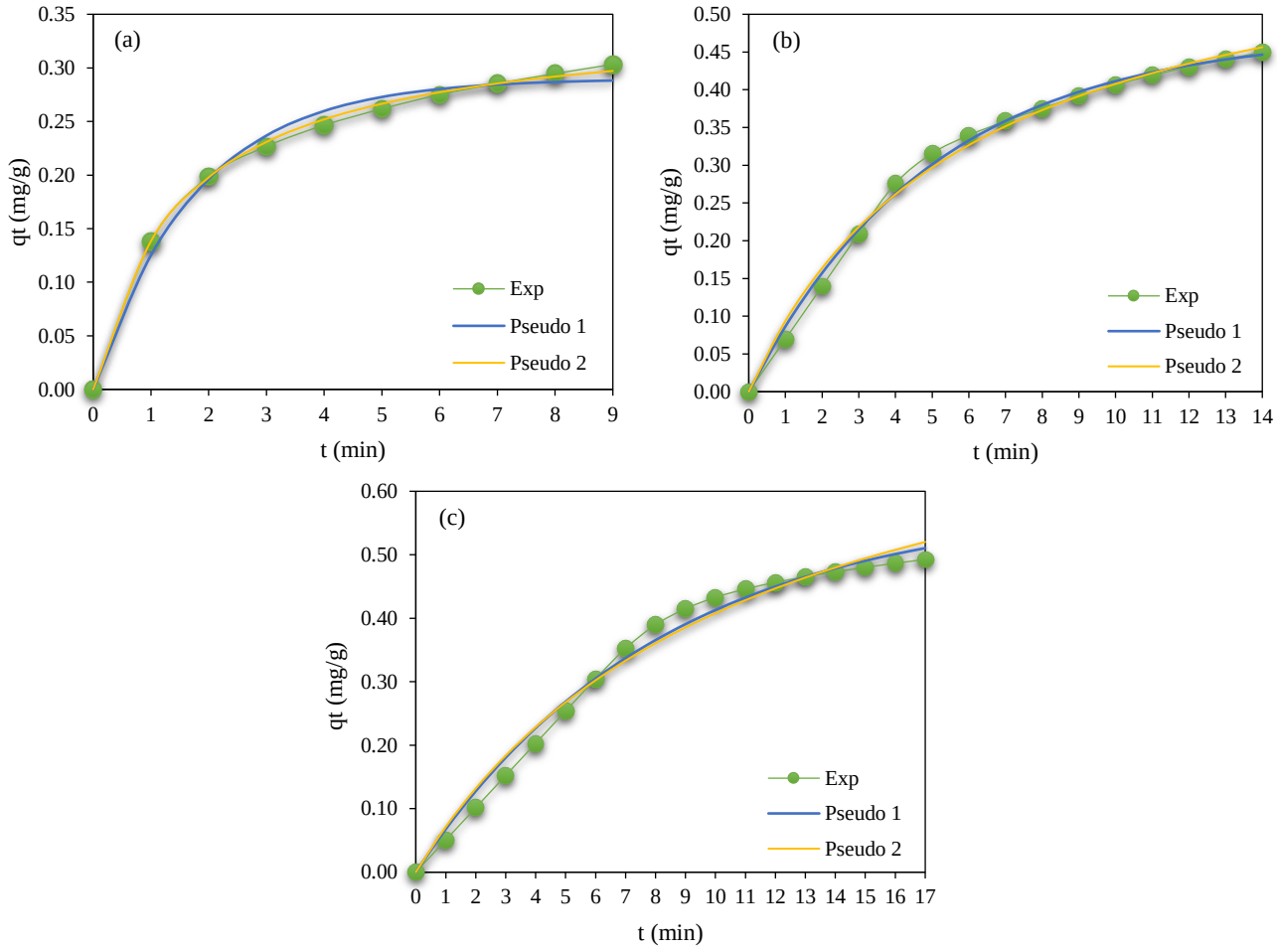

Figure 7. Adsorption kinetics of NH_3 on MP-AC at 20 ppm inlet concentration and adsorbent mass of (a) 1 g, (b) 3 g, and (c) 5 g

3.4.4 Adsorption isotherm

In this study, to describe the interaction between adsorbate and adsorbent at the equilibrium, the Freundlich and Langmuir isotherm were investigated. The linear equation of Freundlich and Langmuir isotherm model is shown in Equation 8 and 9 respectively as follows (Freundlich, 1906; Langmuir, 1917):

$$\log q_e = \log K_F + \frac{1}{n}\log C_e \quad (8)$$

$$\frac{Ce}{qe} = \frac{Ce}{q} + \frac{1}{qK_L} \quad (9)$$

$$R_L = \frac{1}{1+K_L.Co} \quad (10)$$

Where; q_e is the adsorption capacity at equilibrium (mg/g adsorbent), K_F is the Freundlich constant, K_L is the Langmuir constant (L/mg), n is the constant related to the adsorption energy of heterogeneity adsorbent site, Ce is the concentration of contaminants in equilibrium (mg/L), and R_L is equilibrium parameter.

The values of isotherm parameters for both Freundlich and Langmuir isotherm models are presented in Table 4.

Table 4. Isotherm parameters of NH_3 adsorption on MP-AC

Mass	Freundlich				Langmuir			
	1/n	N	K_f (mg/g)(L/mg)$^{1/n}$	R^2	q (mg/g)	K_L (L/mg)	R_L	R^2
1 g	0.195	5.1	0.15	0.615	0.297	820.63	0.09	0.992
3 g	0.153	6.5	1.22	0.644	0.481	611.00	0.12	0.994
5 g	0.146	6.8	1.10	0.877	0.557	544.21	0.13	0.999

Based on determination coefficient (R^2) from Table 4, the Langmuir isotherm is more suitable to describe the NH_3 adsorption process with the R^2 of 0.999. The similar result has also been reported in previous studies for Methylene Blue adsorption (Foo and Hameed, 2012; Nasrullah et al., 2019), and in the NH_3 adsorption on corncob activated carbon (Gebreegziabher et al., 2019). Langmuir isotherms indicates the monolayer adsorption where there is no interaction in adsorbate molecules (El maguana et al., 2020), and the carbon surfaces have homogeneous structures and identical active sites (Kutluay et al., 2019). Moreover, the equilibrium parameter (R_L) value is in the range of $0<R_L<1$, suggesting that the NH_3 adsorption using MP-AC is favorable (Hamzaoui et al., 2018).

4. CONCLUSION

MP-AC prepared from physical activation using CO_2 at 850°C for 120 min shows good porosity with surface area of 588.41 m^2/g, 6.07% moisture content, 9.8% ash content, and iodine number of 1153.69 mg/g. MP-AC can be used as an adsorbent material to remove NH_3 with adsorption capacity of 0.41 mg/g which is lower than commercial activated carbon (0.6-4.7 mg/g). The pseudo-first order kinetic and the Langmuir isotherm are best fitted to the experimental data. Consequently, mangosteen peel may be potentially used as an activated carbon precursor with further modification for NH_3 adsorption and various environmental applications.

ACKNOWLEDGEMENTS

The authors would like to acknowledge Research Center for Nanoscience and Nano-technology ITB for providing facilities in this research.

REFERENCES

Ahmad F, Daud WMAW, Ahmad MA, Radzi R, Azmi AA. The effects of CO_2 activation, on porosity and surface functional group of cocoa (*Theobroma cacao*): Shell based activation carbon. Journal of Environmental Chemical Engineering 2013;1:378-88.

Ahmad MA, Alrozi R. Optimization of preparation conditions for mangosteen peel-based activated carbons for the removal of Remazol Brilliant Blue R using response surface methodology. Chemical Engineering Journal 2010;165:883-90.

Ahmad MA, Alrozi R. Removal of malachite green dye from aqueous solution using rambutan peel-based activated carbon: Equilibrium, kinetic, and thermodynamic studies. Chemical Engineering Journal 2011;171:510-6.

Ambroz F, Macdonald TJ, Martis V, Parkin IP. Evaluation of the BET theory for the characterization of meso and microporous MOFs. Small Methods 2018;2:1800173.

Basrur D, Bhat J. Preparation of activated carbon from mustard seed and its adsorption efficiency towards dye and acid. Journal of Urban and Environmental Engineering 2018; 12:266-76.

Bernal V, Giraldo L, Moreno-Piraján J. Physicochemical properties of activated carbon: Their effect on the adsorption of pharmaceutical compounds and adsorbate-adsorbent interactions. Journal of Carbon Research 2018;4:62.

Chandra TC, Mirna MM, Sunarso J, Sudaryanto Y, Ismadji S. Activated carbon from durian shell: Preparation and characterization. Journal of the Taiwan Institute of Chemical Engineering 2009;40:457-62.

Chen Y, Huang B, Huang M, Cai B. On the preparation and characterization of activated carbon from mangosteen shell. Journal of the Taiwan Institute of Chemical Engineers 2011;42:837-42.

Cheremisinoff PN, Ellerbusch F. Carbon Adsorption Handbook. Michigan, USA: Ann Arbor Science Publishers; 1978.

Choo HS, Lau LC, Mohamed AR, Lee KT. Hydrogen sulfide adsorption by alkaline impregnated coconut shell ativated carbon. Journal of Engineering Science and Technology 2013;8:741-53.

Chung Y, Huang C, Liu CH, Bai H. Biotreatment of hydrogen sulfide- and ammonia-containing waste gases by fluidized bed bioreactor. Journal of the Air and Waste Management Association 2001;51:163-72.

Crini G, Lichtfouse E. Green adsorbents for Pollutant Removal: Innovative material. Heidelberg, Germany: Springer; 2018.

Devi AS, Latif PA, Tham YJ, Taufiq-Yap YH. Physical characterization of activated carbon derived from mangosteen peel. Asian Journal of Chemistry 2012;24:579-83.

Ding S, Liu Y. Adsorption of CO_2 from flue gas by novel seaweed-based KOH-activated porous biochars. Fuel 2020;260:116382.

Domingo-Garcia M, Groszek AJ, Lopez-Garzon FJ, Perez-Mendora M. Dynamic adsorption of ammonia on activated carbons measured by flow microcalorimetry. Applied Catalysis A: General 2002;233:141-50.

El maguana Y, Elhadiri N, Benchanaa M, Chikri R. Adsorption thermodynamic and kinetic studies of methyl orange onto sugar scum powder as a low-cost inorganic adsorbent. Journal of Chemistry 2020;2020:1-10.

Foo KY, Hameed BH. Factors affecting the carbon yield and adsorption capability of the mangosteen peel activated carbon prepared by microwave assisted K_2CO_3 activation. Chemical Engineering Journal 2012;180:66-74.

Fernandez ME, Nunell GV, Bonelli PR, Cukierman AL. Activated carbon developed from orange peels: Batch and dynamic competitive adsorption of basic dyes. Industrial Crops and Products 2014;62:437-45.

Freundlich H. Over the adsorption in solution. Journal of Physics Chemistry 1906;57:385-470.

Gebreegziabher TB, Wang S, Nam H. Adsorption of H_2S, NH_3, and TMA from indoor air using porous corncob activated carbon: Isotherm and kinetic study. Journal of Environmental Chemical Engineering 2019;7:103234.

Ghasemi M, Ghasemi N, Zahedi G, Alwi SRW, Goodarzi M, Javadian H. Kinetic and equilibrium study of Ni(II) sorption from aqueous solutions onto *Peganum harmala*-L. International Journal of Environmental Science and Technology 2014;11:1835-44.

Giraldo L, Moreno-Piraján JC. CO_2 adsorption on activated carbon prepared from mangosteen peel. Journal of Thermal Analysis and Calorimetry 2017;133:337-54.

Guo J, Xu WS, Chen YL, Lua AC. Adsorption of NH_3 onto activated carbon prepared from palm shells impregnated with H_2SO_4. Journal of Colloid and Interface Science 2005; 281:285-90.

Hamzaoui M, Bestani B, Benderdouche N. The use of linear and nonlinear methods for adsorption isotherm optimization of basic green 4-dye onto sawdust-based activated carbon. Journal of Materials and Environmental Sciences 2018; 9:1110-8.

Hastuti N, Pari G, Setiawan D, Mahpudin M, Godang DM. Acidity and alkalinity level of Mayan bamboo activated charcoal (MBAC) on saturated vapor of acid chloride and natrium hydroxide. Widyariset 2015;1:41-50.

Ho YS, McKay G. Pseudo-second order model for sorption processes. Process Biochemistry 1999;34:451-65.

Kang DW, Ju SE, Kim DW, Kang M, Kim H, Hong CS. Emerging porous materials and their composites for NH_3 gas removal. Advanced Science 2020;7:2002142.

Kutluay S, Baytar O, Şahin Ö. Equilibrium, kinetic and thermodynamic studies for dynamic adsorption of benzene in gas phase onto activated carbon produced from *Elaeagnus angustifolia* seeds. Journal of Environmental Chemical Engineering 2019;7:102947.

Lagergren S. About the theory of so-called adsorption of soluble substances. Kungliga Svenska Vetenskapsakademiens Handlingar 1898;24:1-39.

Lan X, Jiang X, Song Y, Jing X, Xing X. The effect of activation temperature on structure and properties of blue coke-based activated carbon by CO_2 activation. Green Processing and Synthesis 2019;8:837-45.

Langmuir I. The constitution and fundamental properties of solids and liquids. II. Liquids. Journal of the American Chemical Society 1917;3:1848-906.

Li Y, Wang X, Cao M. Three-dimensional porous carbon frameworks derived from mangosteen peel waste as promising materials for CO_2 capture and supercapacitors. Journal of CO_2 Utilization 2018;27:204-16.

Meneghetti E, Baroni P, Vieira RS, Da Silva MGC, Beppu MM. Dynamic adsorption of chromium ions onto natural and crosslinked chitosan membranes for wastewater treatment. Material Research 2010;13:89-94.

Mukti NIF, Prasetyo I, Mindaryani A. Preparation of ethylene adsorbent by pyrolysis of mangosteen peels. Proceeding of Indonesian National Seminar on Chemical Engineering 2015 Sustainable Energy and Mineral Processing for National Competitiveness; 2015 Oct 12-13; Gadjah Mada University Club Hotel, Yogyakarta: Indonesia; 2015.

Nasrullah A, Saad B, Bhat AH, Khan AS, Danish M, Isa MH, et al. Mangosteen peel waste as a sustainable precursor for high surface area mesoporous activated carbon: Characterization and application for methylene blue removal. Journal of Cleaner Production 2019;211:1190-200.

Nor NM, Lau LC, Lee KT, Mohamed AR. Synthesis of activated carbon from lignocellulosic biomass and its applications in air pollution control: A review. Journal of Environmental Chemical Engineering 2013;1:658-66.

Nowicki P, Kazmierczak J, Pietrzak R. Comparison of physicochemical and sorption properties of activated carbons prepared by physical and chemical activation of cherry stones. Powder Technology 2015;269:312-9.

Patel H. Fixed bed column adsorption study: A comperehensive review. Applied Water Science 2019;9:1-17.

Rangabhashiyam S, Balasubramanian P. The potential of lignocellulosic biomas precursors for biochar production: Performance, mechanism, and wastewater application. Industrial Crops and Products 2019;128:405-23.

Rattanapan S, Pengjam P, Kongsune P. Preparation and characterization of mangosteen peel activated carbon. Thaksin University Journal 2014;17:13-21.

Reza MS, Yun CS, Afroze S, Radenahmad N, Bakar MSA, Saidur R, et al. Preparation of activated carbon from biomass and its' applications in water and gas purification: A review. Arab Journal of Basic and Applied Sciences 2020;27:208-38.

Ro KS, Lima IM, Reddy GB, Jackson MA, Gao B. Removing gaseous NH_3 using biochar as an adsorbent. Agriculture 2015;5:991-1002.

Saka C. BET, TG-DTG, FT-IR, SEM, iodine number analysis and preparation of activated carbon from acorn shell by chemical activation with $ZnCl_2$. Journal of Analytical and Applied Pyrolysis 2012;95:21-4.

Saputro EA, Wulan VDR, Winata BY, Yogaswara RR, Erliyanti NK. The process of activated carbon from coconut shells

through chemical activation. Journal of Science and Technology 2020;9:23-9.

Statistics Indonesia (BPS). Statistics of Annual Fruit and Vegetable Plants Indonesia 2018. Jakarta, Indonesia: BPS-Statistics Indonesia; 2019.

Unugul T, Nigiz FU. Preparation and characterization an active carbon adsorbent from waste mandarin peel and determination of adsorption behavior on removal of synthetic dye solutions. Water, Air and Soil Pollution 2020;231:538.

Xu R, Tian H, Pan S, Prior SA, Feng Y, Batchelor WD, et al. Global ammonia emissions from synthetic nitrogen fertilizer applications in agricultural systems: Empirical and process-based estimates and uncertainty. Global Change Biology 2019;25:314-26.

Vohra M. Treatment of gaseous ammonia emissions using date palm pits based granular activated carbon. International Journal of Environmental Research and Public Health 2020;17:1519.

Yang T, Lua AC. Characteristics of activated carbons prepared from pistachio-nut shells by physical activation. Journal of Colloid and Interface Science 2003;267:408-17.

Yani M, Nurcahyani PR, Rahayuningsih M. Ammonia removal by biofilter technique packed with coral and granulated activated carbon (GAC) inoculated with enriched nitrifying bacteria. Journal of Agroindustrial Technology 2013;23:22-9.

Yeom C, Kim Y. Adsorption of ammonia using mesoporous alumina prepared by a templating method. Environmental Engineering Research 2017;22:401-6.

Yuliusman, Nasruddin, Afdhol MK, Haris F, Amiliana RA, Hanafi A, et al. Production of activated carbon from coffee grounds using chemical and physical activation method. Advanced Science Letters 2017;23:5751-5.